Probing attractive forces at the nanoscale using higher-harmonic dynamic force microscopy

S. Crittenden,[1,*] A. Raman,[2] and R. Reifenberger[1]
[1]*Department of Physics, Purdue University, West Lafayette, Indiana 47907, USA*
[2]*School of Mechanical Engineering and Birck Nanotechnology Center, Purdue University, West Lafayette, Indiana 47907, USA*
(Received 18 December 2004; revised manuscript received 23 June 2005; published 21 December 2005)

We systematically investigate higher harmonics in the vibration spectrum of scanning force microscope cantilevers operating in the attractive regime. We show that (a) the magnitudes of the higher-harmonic signals in the vibration spectrum should be directly correlated to the local van der Waals forces for systems without significant electrostatic interactions and (b) the higher-harmonic resonances are much sharper than the fundamental harmonic. Consequently, and unlike the case of the tapping mode operation, contrast in the amplitudes of the higher harmonics over a scanned sample with small electrostatic forces reflects changes in specific chemical composition. Dynamic force-distance curves and higher-harmonic images are presented to demonstrate contrast between biological macromolecules deposited on a mica substrate. The results suggest that the systematic measurement of higher harmonics in the attractive regime can lead to highly sensitive techniques to map the chemical composition over heterogeneous samples.

DOI: 10.1103/PhysRevB.72.235422 PACS number(s): 68.37.Ps, 05.45.−a

I. INTRODUCTION

Following its success in nanoscale imaging and metrology, scanning force microscopy (SFM) is being used increasingly for the nanoscale characterization of electronic, mechanical, chemical, and optical properties of a wide variety of materials including metals, semiconductors, polymers, carbon nanotubes, thin films, cells, biological membranes, and biological macromolecules. One of the most widely used SFM methods for measuring the local mechanical properties of the sample such as adhesion, elasticity, or dissipation is dynamic force microscopy (DFM).[1–16] In DFM, the cantilever probe is driven near its first fundamental resonance and its amplitude and phase are monitored as it approaches or retracts from the sample. Several studies have used force-distance,[17–19] frequency shift-distance,[20,21] amplitude-distance,[22] or phase-distance graphs,[23–25] to characterize the local mechanical properties of the sample.

In the pursuit of better quantitative estimation of the nanoscale mechanical properties of the sample, there has been a growing interest in the scanning probe community for the use of higher harmonics in DFM.[26–34] Because the tip-sample interaction forces are inherently nonlinear they modify both the amplitude and phase of the approaching resonating cantilever. In addition, they also generate higher harmonics in the vibration spectrum of the SFM cantilever. If a spectroscopy method can be developed that monitors all the manifestations of these nonlinear tip-sample interaction forces, including higher harmonics, it is likely to identify with greater specificity the tip-sample interaction potential.

Recent work reported in the literature on higher-harmonic dynamic force microscopy has focused on the tapping mode where the tip moves through both the attractive and repulsive regions of the tip-sample interaction in each oscillation cycle (see Fig. 1). Of the two types of interactions, the repulsive interactions which include effects of local sample elasticity are particularly strong in tapping and are expected to be the main driver of higher harmonics. For this reason it is anticipated that the higher harmonics generated during tapping are correlated with the local sample elasticity. Cleveland *et al.* observed the presence of higher harmonics in cantilever oscillations in the tapping mode, but the various frequency components in the spectra were not discussed in any detail.[3] In studies of mechanical properties of samples inferred from tapping mode AFM, Hillenbrand *et al.* obtained dynamic force curves at the 13th harmonic of the cantilever's fundamental resonance.[26] Stark *et al.*[7] showed that the onset of tapping induces increased amplitude at integer harmonics and higher bending modes. Rodriguez and Garcia argued that since higher harmonics are $\sim 10^3$ times smaller than the fundamental mode of oscillation, a linearized equation of motion for the cantilever still remains a good approximation.[35] Stark *et al.* pointed out that higher harmonics tend to provide enhanced sensitivity during the tapping mode scanning probe imaging.[30] They also point out that if higher bending modes closely match an integer harmonic of the cantilever oscillation, higher amplitudes at that harmonic can be excited due to an internal resonance effect. Hembacher and co-workers have demonstrated that higher harmonics provide much enhanced lateral resolution.[36,37] Rodriguez and Garcia have proposed a method[38] for mapping the composition of a surface by exploiting tip-sample nonlinearities and modal interactions in amplitude modulation atomic force microscopy in the attractive regime.

Most of this prior work on higher harmonics has focused on the *repulsive* regime (tapping mode). Higher-harmonic DFM in the *attractive* regime has, to our best knowledge, not been addressed in the literature. An intriguing possibility of higher-harmonic DFM in the attractive regime (Fig. 1) is the quantitative characterization of the local van der Waals forces or Hamaker constants which are a specific indicator of local chemical composition. However, because the attractive van der Waals forces are gentler nonlinearities compared to the strongly nonlinear repulsive interactions, the higher harmonics in the attractive regime are smaller in magnitude than in the tapping mode. In addition, in many cases there may also be electrostatic and electrodynamic (via polarizability of the sample) forces which contribute to the nonlinearities.

 ©2005 The American Physical Society

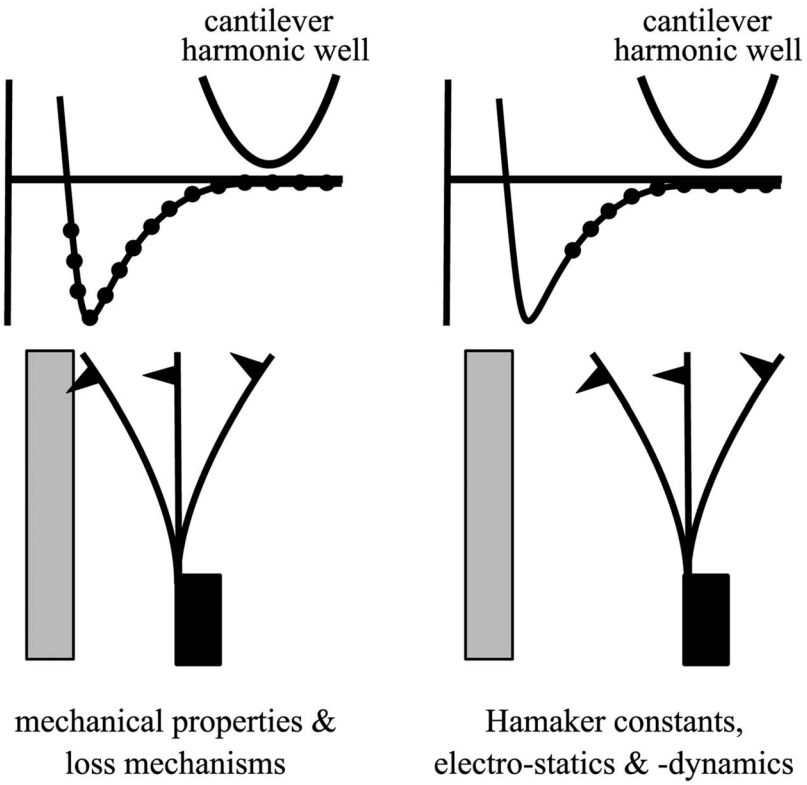

FIG. 1. A schematic diagram showing the tip-substrate interaction potential and the harmonic potential well of the cantilever. In (a) the amplitude of the cantilever is sufficiently large to sample (dotted line) the repulsive regime of the interaction potential. Higher harmonics result due to the non linear interaction of the tip with the substrate. This mode of operation is useful for probing the mechanical properties and loss mechanisms of the tip. In (b), the cantilever oscillation is small enough so that only the tail of the interaction potential (dotted line) is sampled. In this case, higher harmonics are due to distortions in the harmonic well of the cantilever. This mode of operation is useful for probing the Hamaker constant of the substrate.

Thus the measurement of higher harmonics in the attractive regime is more challenging than in the tapping mode, where surface elasticities dominate other contributions, and requires a careful calibration of inherent instrumentation nonlinearities and optimization of the cantilever operating conditions.

We directly address the above issues and present an in-depth study of higher-harmonic DFM in the attractive regime. An application of the technique is illustrated by measuring contrast in higher harmonics over a biological macromolecule—a bilipid membrane—deposited on a mica substrate.

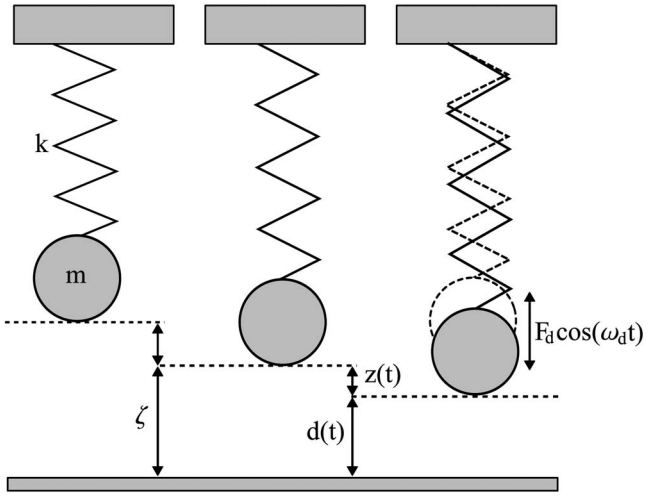

FIG. 2. A description of the parameters involved in the lumped-mass oscillator model of a cantilever (mass m, spring constant k). The cantilever tip responds to an attractive tip-sample interaction potential such that the equilibrium tip-substrate separation distance becomes ς. Additionally, the cantilever is driven at a frequency ω_d which is near the first natural bending mode frequency $\omega_{B1} = \sqrt{k/m}$.

II. THEORETICAL CONSIDERATIONS

In this section we briefly provide a mathematical treatment of a simple model for a SFM tip oscillating in the attractive regime that demonstrates the dependence of higher harmonics on the local nonlinearity. Specifically our discussion follows along the lines of prior studies that have dealt with single-degree-of-freedom models oscillating in a non-quadratic potential well.[7,26–28,30,35,38–40] We consider the case where the only force present is due to the van der Waals interaction between the tip and sample. We also use a more general interaction force law valid for large tip-substrate separations.

In this single-degree-of-freedom model (Fig. 2), the cantilever is modeled as a simple harmonic oscillator of linear stiffness k, and lumped mass m, that interacts with the substrate through nonretarded van der Waals forces. This simple system models approximately the dynamics of the first bending mode of the microcantilever with a resonant frequency ω_{B1}. If the instantaneous gap between the tip and the sample is $d(t)$, the attractive van der Waals force between a sphere of radius R (tip) and a half space (substrate) is known to be[17] of the form (valid for arbitrary d):

$$F_{tip\text{-}sample}(d) = \frac{2HR^3}{3d^2(2R+d)^2} \tag{1}$$

where H is the local Hamaker constant between the spherical tip and the substrate. As the tip is brought close to the sub-

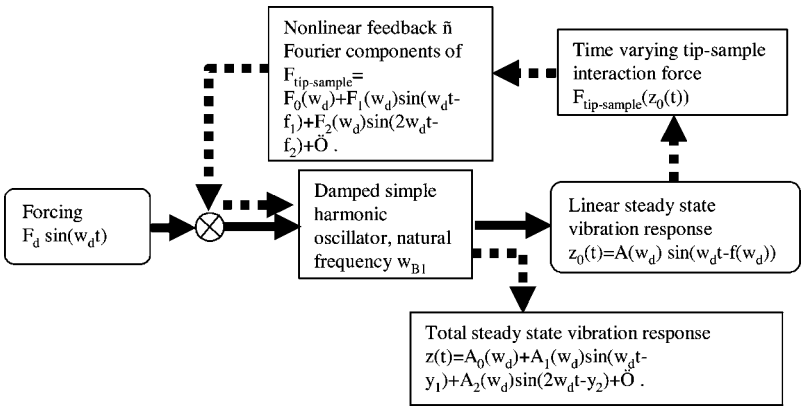

FIG. 3. A schematic of the analytical approximation technique used to compute the magnitudes of the higher harmonics. The method is based on the describing function technique used in the nonlinear systems community (Refs. 39 and 40) and follows along the lines of other researchers (Ref. 30). The dashed arrow represents the nonlinear feedback mechanism while the solid arrows represent the linear dynamics.

strate it deflects statically under the action of the van der Waals force until it reaches an equilibrium tip-substrate separation ς. The cantilever is now excited mechanically with a sinusoidal force $F_d\cos(\omega_d t)$, deflecting the probe tip a distance $z(t)$ from its equilibrium position. The equation of motion of the probe tip in its equilibrium position damping constant c, using the interaction force (1) can then be written as

$$m\ddot{z} + c\dot{z} + kz = F_{tip\text{-}sample}(z) + F_d \sin(\omega_d t),$$

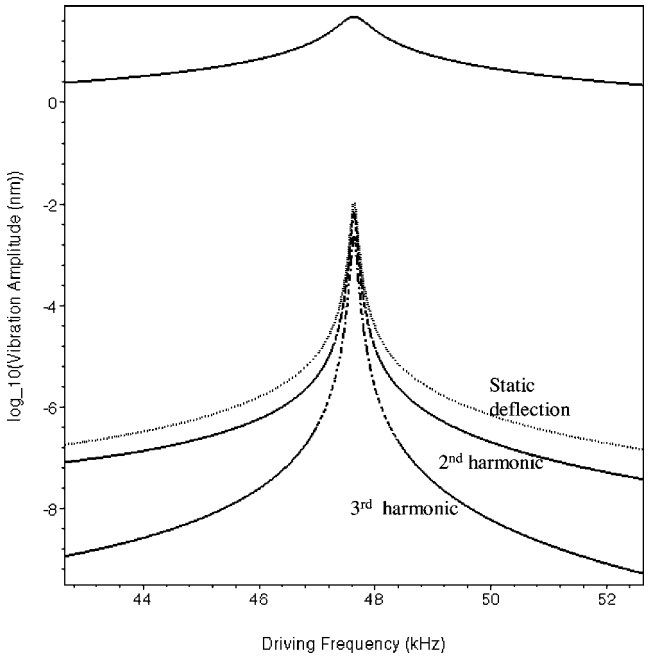

FIG. 4. Driving frequency dependence of the higher and zeroth (static deflection) harmonics for a cantilever with a first bending mode frequency $\omega_{B1}=47.64$ kHz. The curves are predicted by the describing function approach for the nominal system parameters listed in the text. Note that the shape of the higher harmonic resonances is progressively sharper than the fundamental harmonic response plotted at the top of the figure. When driven at resonance, the amplitude of the second harmonic is predicted to be ~3 orders of magnitude below the first bending mode resonance amplitude.

$$F_{tip\text{-}sample}(z) = \frac{2HR^3}{3(\varsigma - z)^2(2R+\varsigma - z)^2} - \frac{2HR^3}{3\varsigma^2(2R+\varsigma)^2}$$

$$\Rightarrow \ddot{z} + \frac{\omega_{B1}}{Q}\dot{z} + \omega_{B1}^2 z = \varepsilon\left(\frac{1}{\left(1-\frac{z}{\varsigma}\right)^2\left(1-\alpha\frac{z}{\varsigma}\right)^2} - 1\right) + \frac{F_d}{m}\sin(\omega_d t)$$

$$\varepsilon = \frac{2}{3}\frac{HR^3}{m\varsigma^2(2R+\varsigma)^2}, \quad \alpha = \frac{\varsigma}{2R+\varsigma}, \tag{2}$$

where

$$\varepsilon = \frac{2}{3}\frac{HR^3}{m(2R+\varsigma)^2} = \frac{2}{3}\frac{\omega_{B1}{}^2 HR^3}{k(2R+\varsigma)^2}$$

is a natural small parameter that is a measure of the cantilever tip acceleration caused by the van der Waals attractive force on the spherical tip when the tip is placed at a distance ς from the sample. The geometrical parameter $\alpha=\varsigma/2R+\varsigma$ describes how the tip-sample equilibrium separation is related to the tip radius. Furthermore $\omega_{B1}=\sqrt{k/m}$ is the undamped natural resonance frequency of the first bending mode, and Q is the corresponding Quality factor.

Moving towards the goal of deriving simple expressions for the higher-harmonic amplitudes, we note that the nonlinearity in the driven oscillator Eq. (2) is scaled by the small parameter ε. Accordingly the nonlinearity is weak and we will resort to an approximation known as the describing function technique which is often used in the literature of the control of nonlinear systems.[41,42] According to this technique, the output $z(t)$ of this weakly nonlinear system [Eq. (2)] can be approximated by regarding the effect of the nonlinearity as an additional feedback $[z_1(t)]$ on the otherwise linear dynamic system. Figure 3 provides a schematic diagram that illustrates the basic principles involved. This approach is used by other researchers[7,16,26,30] that deal with higher harmonics, however, our case is specialized to the attractive regime of operation with exact expressions of sphere-plane interaction potential.

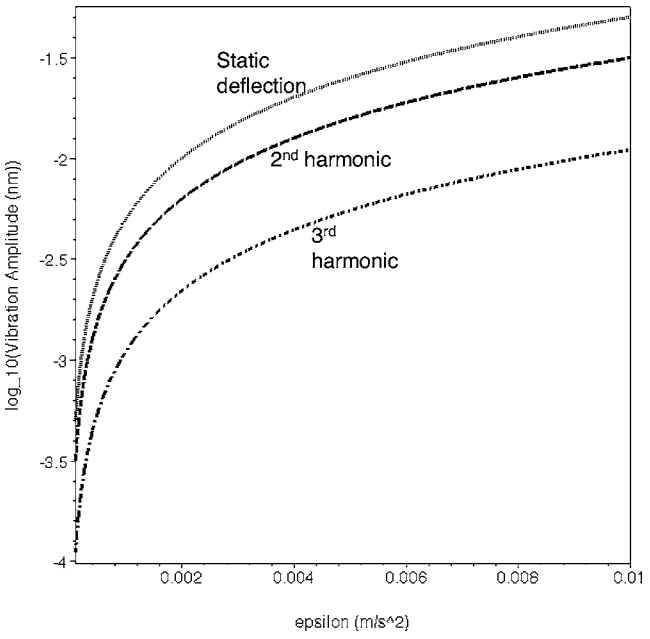

FIG. 5. Variation of the amplitudes of the second, third, and zeroth (static deflection) harmonics of vibration as a function of the parameter ε (that is linearly proportional to the local Hamaker constant). These calculations are performed for nominal lumped system values stated in the text and when $\omega_{\mathrm{d}}=\omega_{\mathrm{B1}}$.

Accordingly, we substitute $z(t)=z_0+\varepsilon z_1+O(\varepsilon^2)$ into Eq. (2) and equate terms that are independent of ε thus yielding the underlying linear dynamic system whose steady state (particular) solution is known to be (see Fig. 3)

$$z_0(t) = A\,\sin(\omega_d t - \phi),$$

$$A(\omega_d) = \frac{F_d/k}{\left(\left[\left(\frac{\omega_d}{\omega_{B1}}\right)^2 - 1\right]^2 + \left(\frac{1}{Q}\frac{\omega_d}{\omega_{B1}}\right)^2\right)^{1/2}},$$

$$\phi(\omega_d) = \tan^{-1}\left(\frac{1}{Q}\frac{\omega_d/\omega_{B1}}{(\omega_d/\omega_{B1})^2 - 1}\right). \tag{3}$$

In order to compute the first order correction term $z_1(t)$, we collect terms of $O(\varepsilon)$ when $z(t)=z_0+\varepsilon z_1+O(\varepsilon^2)$ is substituted into Eq. (2):

$$\ddot{z}_1 + \frac{\omega_{B1}}{Q}\dot{z}_1 + \omega_{B1}^2 z_1 = \frac{1}{\left(1-\frac{z_0}{s}\right)^2\left(1-\alpha\frac{z_0}{s}\right)^2} - 1$$

$$= F_0(\omega_d) + \sum_{n=1}^{\infty} F_n(n\omega_d)\sin(\omega_d t - \phi_n) \tag{4}$$

so that the solution of the leading order term (3) appears in the nonlinear feedback forcing on the right-hand side of (4). The nonlinear feedback forcing term in turn can be expanded as a Fourier series containing integer harmonics $(n\omega_d)$ of the driving frequency with parameters F_n and ϕ_n that are easily evaluated using symbolic mathematics software such as MAPLE or Mathematica. The steady state solution of the linear system (4) to nonlinear feedback can be then written as

$$z_1(t) = A_0 + \sum_{n=1}^{\infty} A_n \sin(n\omega_d t - \psi_n),$$

$$A_0 = \frac{F_0}{{\omega_{B1}}^2}, \quad A_n = \frac{F_n/{\omega_{B1}}^2}{\left(\left[\left(\frac{n\omega_d}{\omega_{B1}}\right)^2 - 1\right]^2 + \left(\frac{n}{Q}\frac{\omega_d}{\omega_{B1}}\right)^2\right)^{1/2}},$$

$$\psi_n(\omega_d) = \phi_n + \tan^{-1}\left(\frac{1}{Q}\frac{n\omega_d/\omega_{B1}}{(n\omega_d/\omega_{B1})^2 - 1}\right) \tag{5}$$

and the overall steady state response of the oscillator takes the form

$$z(t) = A(\omega_d)\sin(\omega_d t - \phi) + \varepsilon\left(A_0(\omega_d) + \sum_{n=1}^{\infty} A_n^s(\omega_d)\right.$$

$$\left.\times\sin(n\omega_d t - \psi_n) + A_n^c(\omega_d)\cos(n\omega_d t - \psi_n)\right). \tag{6}$$

Clearly, the nonlinear tip-sample interaction forces not only modify the gain and phase of the response at the driving frequency ω_d, but they also cause a static deflection $\varepsilon A_0(\omega_d)$ (zeroth harmonic) and generate higher harmonics in the vibration spectrum. Further, the amplitude of the higher harmonics is linearly proportional to the value of the local Hamaker constant H through the parameter ε.

Let us consider a specific numerical example where the parameters are chosen to reflect typical values that are encountered in the experiments to be presented shortly. The parameters chosen include the first bending mode cantilever frequency $\omega_{\mathrm{B1}}=47.64$ kHz, $\zeta=50$ nm, $k=1.1$ N/m, $R=20$ nm, $H=100$ zJ, $Q=100$, and $F_{\mathrm{d}}=5.37\times10^{-10}$ N. The corresponding value of $\varepsilon=2.14\times10^{-3}$ ms^{-2}. In the absence of the tip-sample interaction, the vibration amplitude is 48.8 nm. The magnitudes of the zeroth, primary, secondary, and tertiary harmonics were calculated using the method described earlier using MAPLE. Figure 4 shows the dependence of the different harmonics on the driving frequency ω_d. In Fig. 5 the variation in the magnitudes of the second and third harmonics and static deflection are plotted as a function of the driving frequency and the parameter ε which is directly proportional to the Hamaker constant H.

Four clear observations can be made from this calculation. First, the magnitudes of the second harmonic and static deflection are $\sim$3 orders of magnitude lower than the response at the fundamental bending mode of the cantilever, consistent with theoretical and observational reports of other workers. The magnitude of the third harmonic is even smaller than the second and the zeroth harmonic. Secondly, the magnitudes of these harmonics increase linearly with the increase of the local Hamaker constant [Eq. (6)]. Thirdly, a small shift in the value of ω_{B1} due, for example, to the tip-substrate interaction is magnified by a factor of n for the nth harmonic of ω_{B1}. In this sense the frequency shifts of the

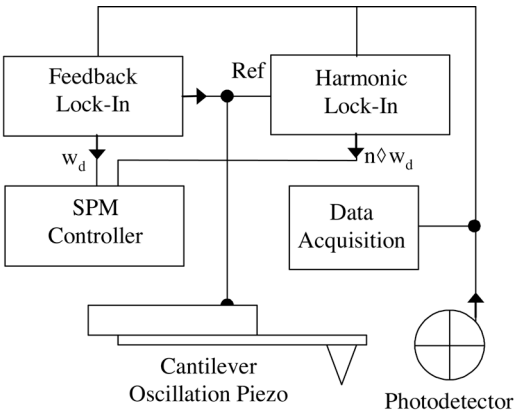

FIG. 6. Schematic of the experimental apparatus. The signal from the position sensitive photodetector is simultaneously digitized by a data acquisition module and measured by two lock-in detectors. The harmonic lock-in uses the reference signal to extract the *n*th harmonic from the photodector signal, which is then plotted as a function of position by the Nanotec SPM controller. The feedback lock-in measures the component of the photodetector signal at the piezo drive frequency ω_d, which is then plotted to provide a topographic image by the Nanotec SPM controller in the usual way.

higher harmonics are much more sensitive to van der Waals forces than the first harmonic.

Lastly, the response of the higher harmonics is much "sharper" than the response at the fundamental bending mode resonance. Essentially, the higher the harmonic, the sharper the resonance peak. This is inherently due to the nonlinearities of the problem and can be explained as follows. The amplitude of the linear response $A(\omega_d)$ can be described by a typical Lorentzian resonance peak. If a higher harmonic signal could somehow be fed back into a *linear* tip-substrate interaction, any resulting higher harmonic would have the same shape as $A(\omega_d)$. However, since the feedback response is really *non linear*, the higher-harmonic response is scaled by the nonlinearity, resulting in the successive sharpening of the higher-harmonic peaks. It follows that the increasing sharpness of the higher-harmonic peaks cannot be interpreted in terms of a reduction in dissipation.

When discussing experimental results, it is worthwhile to distinguish between the *higher harmonics* and the *higher modes* of a microcantilever. For vibrating strings, the natural frequencies of different string higher modes happen to be consecutive integer multiples, or harmonics, of each other, thus forming the natural octaves of musical instruments. In the vibrations of beams, however, the frequencies of the different modes are not ordered as consecutive harmonics. In fact in the classical Bernoulli-Euler beam theory, the frequency of the second bending mode is ~6.27 times that of the first. For vibrating beams, therefore, the one-to-one analogy between higher modes and harmonics breaks down. The higher harmonics that we refer to in this paper are the higher harmonics of the forcing signal that are due to the nonlinear interactions between the tip and the sample, and cannot be understood with linear vibration theory. In what follows, we will refer to the driving harmonic as ω_d, and its higher harmonics as $n\omega_d$. The different natural vibration modes of the cantilever will be classified as B1, B2, etc. corresponding to the first, second, and higher bending modes. The corresponding natural frequencies are then ω_{B1}, ω_{B2}, etc. In practice, $\omega_d \approx \omega_{B1}$

We note that if we had instead assumed an electrostatic origin of the tip-sample force[43] the detailed formulas for ε would depend directly on a scale factor representing the magnitude of the potential difference. We would still be able to extract, not H, but, what would be its equivalent, a single number giving a scale to the interaction potential. However, if we assume both van der Waals and electrostatic components to the force, the describing function method yields an "effective" ε that is a convolution of the electrostatic potential difference, the Hamaker constant, and the various geometric parameters involved (z, R, zeta, etc.).

Nevertheless, this theoretical analysis provides a simple understanding of the origin of higher-harmonics and provides a basis for higher-harmonic dynamic force microscopy in the attractive regime. The utility of this method lies in the relationship of the higher harmonics to local Hamaker constants through the parameter ε, assuming that local electrostatic forces can be minimized. In what follows we describe detailed experimental results using higher-harmonic dynamic force microscopy that confirm many of the predictions inherent in the model presented above.

III. EXPERIMENTAL SETUP

Cantilevers from multiple manufacturers of various shapes and stiffnesses were used to investigate higher-harmonics phenomena. By far the best results were obtained using Ultrasharp NSC12 F rectangular cantilevers with aluminum back-coating from Mikromasch, Inc. Unless otherwise specified, data in this paper is from a single, particular, cantilever with measured natural fundamental bending frequency $\omega_{B1}=47.64$ kHz and interpolated $k=1.1$ N/m. In general, the second bending mode frequency ω_{B2} depends on the detailed shape and material properties of the cantilever. It is therefore possible to design cantilevers for which ω_{B2} is very close to $n \times \omega_{B1}$. This frequency tuning is referred to as internal resonance. For the Mikromasch NSC12 F cantilevers used in this study, ω_{B2} usually happens to be within 5% of $7\omega_{B1}$; most of the data presented here are from the cantilever referenced above for which $\omega_{B2} \cong 7.00\ \omega_{B1}$.

All data were acquired with an ambient air SFM from Nanotec Electronica™ operating in the dynamic mode. A schematic of the experimental setup is given in Fig. 6. Two external lock-ins from Signal Recovery, Inc. (Models 7280/99 & 7280/98) were used, one to mechanically oscillate the cantilever at variable frequency ω_d and to extract amplitude and phase information in real time for SPM feedback, and the second to do the same for higher harmonics of the driving frequency. The angle between the cantilever and the substrate has a large effect on the measured higher harmonics, whose amplitude scales roughly as the cosine of the angle. Therefore, the SFM head was adjusted until the cantilever was almost flat with respect to the sample (cantilever-sample angle $< 5°$), in order to give the largest signals.

The ambient humidity also noticeably affects higher-harmonics signals. We conjecture that this may be due to

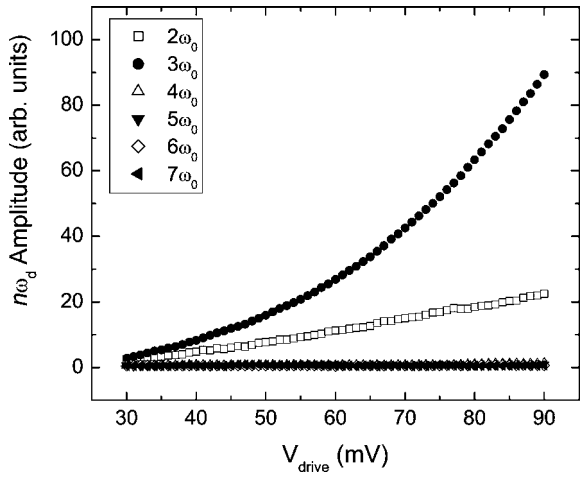

FIG. 7. Spurious higher-harmonic signals can be generated when the cantilever is far from the substrate if the cantilever is overdriven. These higher harmonics occur in the absence of any tip-sample interaction and are probably due to a variety of causes like a small distortion in the driving signal, photodetector and other optical system nonlinearities, or nonlinear damping from the surrounding air. This is a plot of the measured amplitudes for an NSC12 F cantilever at different harmonics $n\times\omega_d$, $n=2-7$, as a function of the driving voltage to the dither piezo when $\omega_d\cong\omega_{B1}$. Below a dither voltage of ~30 mV (corresponding to ~40 nm peak-to-peak oscillation at ω_d), negligible higher harmonics are generated. Above a dither voltage of ~30 mV the amplitude of oscillation observed at $2\omega_d$ and $3\omega_d$ increases and is clearly much larger than the other higher harmonics. The response at $3\omega_d$ is noticeably nonlinear and larger than at $2\omega_d$ due primarily to optical system nonlinearities. $7\omega_d$ is small here because it is only strongly excited when interacting with the sample.

capillary formation or extensive surface water layers at higher humidity. Therefore, unless otherwise specified, all data presented below were acquired at a low relative humidity of ~5% obtained by continuous flushing of the SFM with a high purity dry nitrogen gas. There was a need to adjust the SFM optics after dehumidifying so the standard bell jar used to isolate the SFM from the ambient atmosphere was replaced with a clear plastic bag to allow access to adjustment screws while maintaining a dry environment.

Finally, a high speed data acquisition system (two National Instruments NI-5911 5MS/s cards in a standard PC) was used to capture both the driving signal and the cantilever oscillation at 2.0–2.5 MS/s.

IV. OPTIMIZATION OF EXPERIMENTAL FACTORS

In this section we discuss several experimental factors that required systematic optimization and control in order to achieve reasonable and repeatable measurements of the higher harmonics. Many of these factors are not normally considered when collecting data with the SFM.

A. Humidity and capillary forces

Experimentally, it was found much easier to obtain sizeable second-harmonic signals at ambient humidity. In addition, many cantilevers display a distinctly nonsinusoidal oscillation when near the substrate at high humidity. It is well known that at an appreciable humidity, water necks can form between the tip and sample during non-contact and tapping mode imaging.[13,44–46] To reduce the possibility that water necks formed when the cantilever was close to the sample, the humidity was reduced to ~5% relative humidity, held at this level for ~20 min before the data acquisition and kept at this level throughout the measurement.

B. Spurious harmonics and laser positioning

When the reflected laser is properly aligned on the photodetector, the amplitude of the second harmonic remains unchanged until the first harmonic amplitude begins to decrease due to tip-substrate interaction, at which point the second harmonic generally increases. This follows the theoretical model presented in the previous section. If, however, the laser spot is poorly aligned on the photodetector (with all other experimental parameters fixed; cantilever, relative humidity, and driving amplitude) the second harmonic amplitude instead decreases when the tip approaches the sample. At an intermediate state of alignment, where the laser is just a little off from its optimal position, the second harmonic amplitude starts to decrease when the first harmonic amplitude decreases, but subsequently increases as the tip comes closer to the sample. The fact that these effects can be induced or suppressed by adjusting the laser spot on the photodetector, strongly suggests they are due to optical detection system nonlinearities. Following this careful investigation of the effects of laser positioning, the laser spot position was controlled in all subsequent experiments to ensure appropriate behavior of the higher harmonics.

In addition to the artifacts induced by laser alignment in the photodetector, spurious harmonics can be generated by imprecise positioning of the laser on the cantilever.[47–50] For instance, it was found that when a significant portion of the laser illumination is off the edge of the cantilever, light reflected from the substrate interfered constructively and destructively in the photodetector with the light reflected from the cantilever. This led to spatial variations in intensity over the photodetector. These variations occur at half the wavelength of the laser. Because the sample-cantilever angle is small, this interferometric effect can be large. Particular care was taken in the experiments to avoid this situation as the harmonic signals from the tip-sample interaction are 1000 times smaller than the fundamental.

C. Driving amplitude dependence

Once the relative humidity and laser positioning were carefully adjusted based on the discussion above, a systematic study of the effects of driving amplitude on higher-harmonics generation was performed. For instance, Fig. 7 shows the variation of higher-harmonic amplitudes with driving amplitude for the experimental cantilever, when ω_d is within 10 Hz of its first bending frequency ω_{B1}. These data were acquired when the cantilever is far from the substrate. Figure 7 shows that once the first bending mode amplitude increases beyond ~40 nm peak to peak, measurable higher

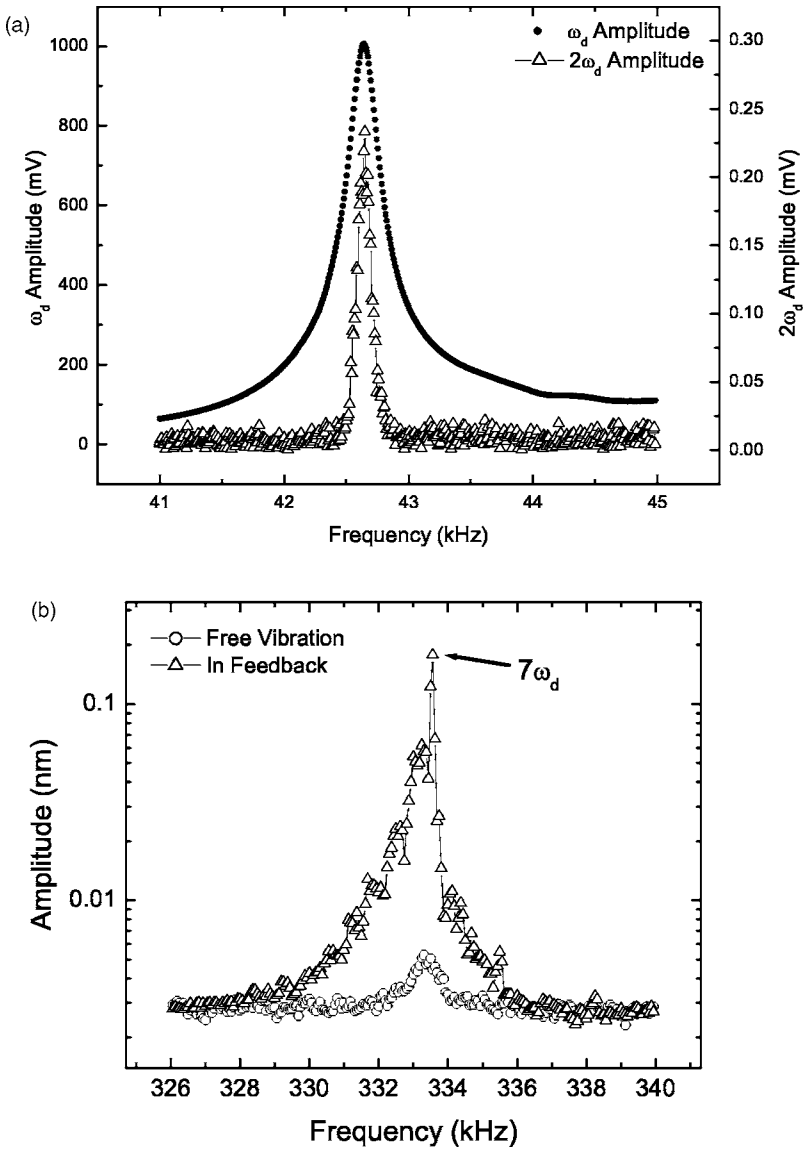

FIG. 8. In (a), simultaneously acquired resonance peaks as ω_d is varied for a representative NSC12 F cantilever. The resonance at $2\omega_d$ is sharper than at ω_d. As the tip approaches the substrate, both peaks shift to lower frequencies; since the second harmonic resonance is sharper, any shift in frequency will generate a larger response. In (b) a plot of the thermal (undriven) resonance at ω_{B2} far from the substrate. When the tip is driven at $\omega_d = \omega_{B1}$ and approaches the substrate, the resonance at ω_{B2} broadens and a sharp resonance peak appears at $7\omega_d$.

harmonics appear in the vibration spectrum. These occur in the absence of any tip-substrate interaction and are probably due to a variety of causes such as small distortions in the driving signal, photodetector, or other optical system nonlinearities, or nonlinear damping from the surrounding fluid. Driving the cantilever too hard produces significant higher-harmonic signals which can mask the small contributions due to differences in interaction force from the substrate. Accordingly the drive amplitude was adjusted in subsequent experiments to ensure that the free-space first bending mode amplitude was ~40 nm peak to peak to minimize spurious higher harmonic signals.

D. Driving frequency dependence

In performing standard dynamic force-distance curves, it is usually possible to set the driving frequency to match the first bending frequency, or lie just below, or just above it without much care. However, special attention needs to be exercised if measurements involving higher harmonics are of interest. To demonstrate this, Figure 8(a) shows the magnitude of the photodetector output as ω_d is swept through the first bending frequency ω_{B1}. Also plotted is the photodetector response at the second harmonic $(2\omega_d)$ of an NSC12 F cantilever as the driving frequency is swept through ω_{B1}. Clearly, the resonance curve is considerably sharper for the second harmonic than it is for the first harmonic, in qualitative agreement with the predictions of the model outlined in Sec. II. Figure 8(b) shows a similar plot for data taken around the second bending mode frequency, which for this cantilever is very close to $7\omega_d$. The undriven (thermally excited) cantilever shows a weak signal corresponding to the ω_{B2} resonance. When the cantilever is driven through ω_{B1}, a very sharp resonance corresponding to $7\omega_d$ appears. Again, the resonance at higher harmonics is considerably sharper than the more familiar resonance of the cantilever at ω_{B1}.

It follows from this discussion that in order to maximize the higher-harmonic signals, care must be taken in choosing a driving frequency ω_d. All subsequent data were acquired by setting the driving frequency within 10 Hz of ω_{B1}.

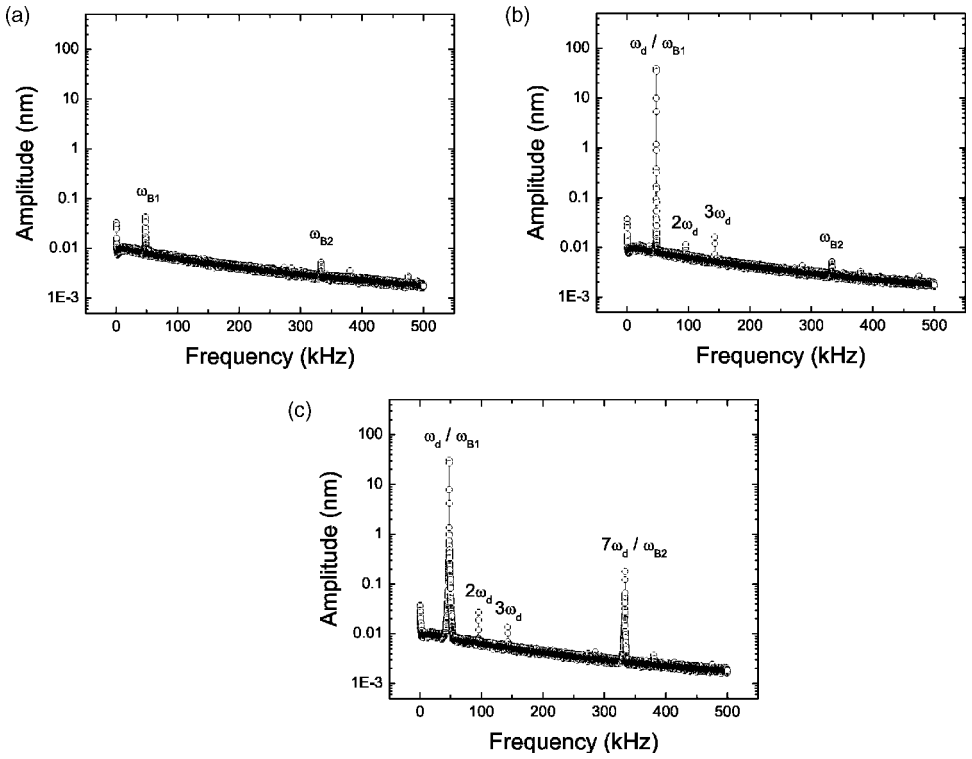

FIG. 9. Frequency spectra for a Mikromasch NSC12 F cantilever (ω_{B1}=47.64 kHz). As discussed in the text, the vertical scale has an arbitrary normalization for peaks other than at the first bending mode. (a) Undriven response far from the substrate. Thermal excitation of the first and second bending modes is apparent. Small additional peaks are of unknown origin. (b) Driven response far from the substrate with $\omega_d \cong \omega_{B1}$. The amplitude of the ω_{B1} mode is ~40 nm peak-to-peak. Peaks at $2\omega_d$ and $3\omega_d$ due to small system nonlinearities are now visible. The response at ω_{B2} is largely unaffected. (c) Noncontact mode (attractive regime) near a mica substrate with $\omega_d \cong \omega_{B1}$. The peaks at $2\omega_d$ and $3\omega_d$ have changed and the response at $\omega_{B2}/7\omega_d$ is much larger.

E. Calibration of higher harmonic and higher mode signals

The output from the photodetector is proportional not directly to the tip deflection but rather to the slope of the cantilever near the tip. It is customary therefore to assume a certain deflection profile for the cantilever which then provides a prescription of the relationship between tip deflection and tip slope. This prescription can be used together with knowledge of the photodetector sensitivity to convert the photodetector voltage output into tip deflection. Usually, during a calibration, the shape of the cantilever is either chosen to be its deflection profile under a static tip load, or its first bending mode shape. It is known that calibrations based on these two methods differ by ~10%.

However it is not immediately obvious whether either of the above customary calibration procedures can be used to correctly measure the amplitudes of the higher harmonics. To understand this we take recourse to the theory of nonlinear oscillations for continuous structures.[39] It is known in the nonlinear vibrations literature that if a beam subject to weakly nonlinear restoring forces is driven near a resonance, the nonlinearity is manifest not in the mode shape but rather in the temporal dynamics of the mode shape. This situation is precisely what one encounters in the attractive regime. Therefore, when the cantilever is driven at its fundamental bending resonance, its shape corresponds to its fundamental mode shape while its temporal dynamics may show higher harmonics. In light of this argument, it is clear that the customary calibration methods can be used to measure the magnitude of the higher-harmonic signals. Accordingly, the static deflection calibration is applied to all the measured data.

Finally, as a word of caution, we note that for cantilevers with internal resonances such as those used in this study, a certain harmonic of the primary resonance interacts strongly with higher order modes of the beam.[49] Because the mode shapes of these higher order modes are very different from the fundamental bending mode, it is difficult to calibrate the harmonic that interacts strongly with a higher order mode. In the present work, the seventh harmonic interacts strongly with the second bending mode of the cantilever. However, in the present study we use the same calibration for the seventh harmonic as we do for all the other harmonics. For this reason, quantitative estimates for amplitudes, etc. must be treated with caution.

F. Thermal and driven spectra

Prior to investigating higher-harmonic dynamic force microscopy, the thermal and forced vibration spectrum of the cantilever is described. In order to measure these spectra, all unnecessary equipment in the room including lighting was turned off as investigations showed that some equipment contributed to measurable spurious signatures in the spectra. Figure 9(a) shows the power spectrum of a thermally driven

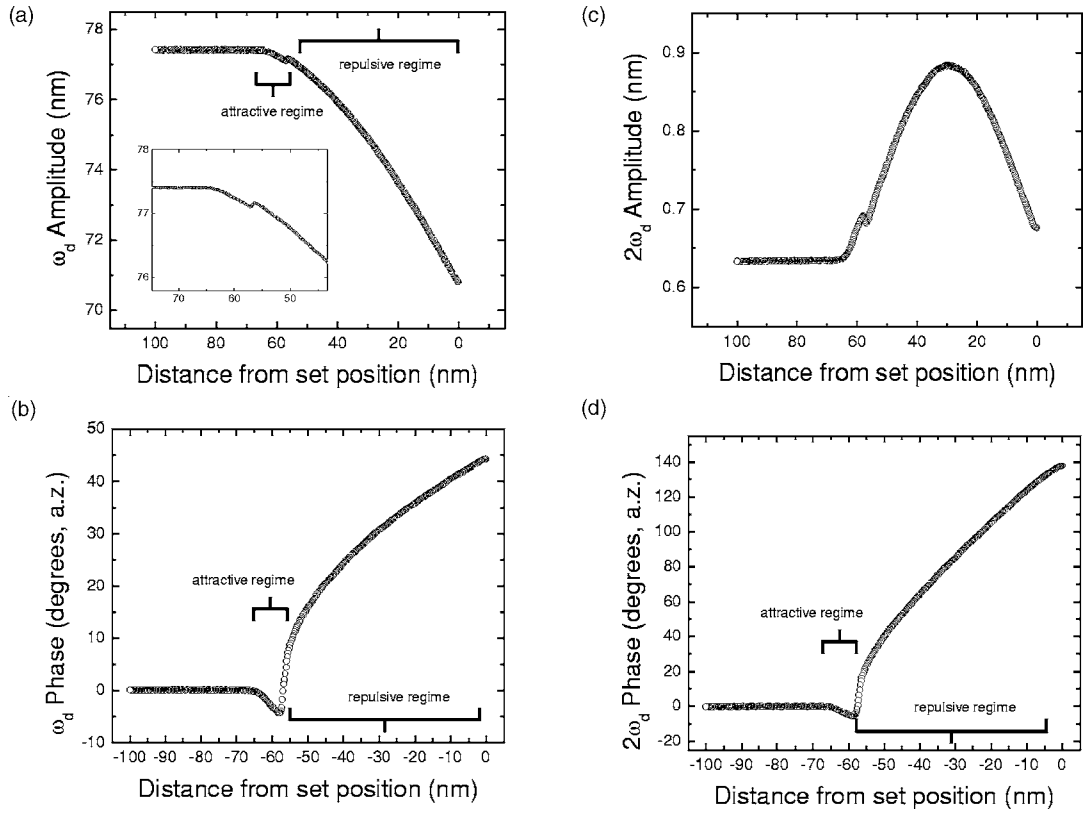

FIG. 10. First and second harmonic variations as a function of tip and/or substrate separation showing both amplitudes (a) and (c) and phase change (b) and (d) for an NSC12 C cantilever when $\omega_d \cong \omega_{B1}$. All data were acquired simultaneously to ensure accurate comparison between the various features of interest. Note that the amplitude of the second harmonic begins to increase at the same tip and/or substrate separation as the amplitude of the fundamental begins to decrease. The transition between the attractive and repulsive mode produces a well-defined jump in the amplitude as well as a change in the slope for the phase. The inset in (a) is a close-up of the transition. All curves are averages of five dynamic force-distance curves, indicating a high degree of repeatability.

cantilever far from a substrate when the data are sampled at 4 MHz. There are clear peaks at both first and second bending frequencies due to thermally induced vibrations at these frequencies; interestingly, the location of the thermal peak does not occur at the same frequency as the driven resonance. This data can be used to calibrate the cantilever spring constant.[51,52]

Figure 9(b) shows the spectrum when the cantilever was driven to oscillate with ~40 nm peak-to-peak amplitude far away from the substrate. There are small peaks indicating the presence of higher harmonics of the driving frequency, in addition to the thermally excited second bending mode frequency at ω_{B2}. The fact that higher harmonics are generated even before the tip approaches the substrate is attributed to remaining nonlinearities in the system optics and electronics as discussed above.

Figure 9(c) shows a typical spectrum when in the attractive regime of the substrate. The tip-substrate interaction clearly changes the forced vibration spectrum of the cantilever. Several harmonics are now seen with the seventh harmonic and/or second bending mode clearly dominating. The simple theoretical model presented earlier cannot predict this result because it does not consider the interaction between the seventh harmonic and the second bending frequency. These results are fairly repeatable for all the Mikromasch NSC12 F cantilevers tested.

G. Distinguishing between attractive and repulsive regime DFM

In order to perform dynamic force-distance curves using higher harmonics, it is necessary to first determine whether the cantilever is operating in the repulsive or attractive regime. This is accomplished in the usual way[12] by monitoring the phase of the cantilever oscillation as it approaches the sample. Figure 10 shows the variation in the amplitude and phase of the first bending mode and its second harmonic with approach distance. This measurement was made with the experimental cantilever using fixed excitation amplitude over freshly cleaved highly oriented pyrolytic graphite at low (~5%) relative humidity. The change in the sign of the phase indicates the transition from the attractive to the repulsive regime. This criterion was used to ensure that all subsequent data are measured in the attractive regime.

V. INVESTIGATIONS OF BACTERIORHODOPSIN/PURPLE MEMBRANE

A number of studies were performed in order to determine the utility of the higher-harmonic dynamic force microscopy to resolve attractive interaction-potential differences in heterogeneous samples. Since the technique is of high interest in studies of biological macromolecules, our initial studies

were performed on the purple membrane (PM). In what follows, the sample preparation methods and experimental results are described.

A. Sample preparation

Purple membrane was chosen for this study because it is known to be quite robust and easy to deposit in submonolayer amounts. Patches of PM are known to be comprised of the protein bacteriorhodopsin embedded periodically in a bilipid membrane. The PM patches are ~200 nm in diameter and ~5 nm high. Wild type purple membrane (WT PM) in distilled water, concentration ~1 mg/mL, was diluted by a factor of 20 with MilliPore™ deionized water. 10 μL of the dilute solution was deposited on freshly cleaved mica and allowed to dry in an enclosed Petri dish under ambient laboratory conditions. This concentration was chosen to ensure a convenient percentage of PM surface coverage while also leaving large open areas of mica to allow unambiguous determination of bare substrate levels and orientation.

B. Higher harmonic imaging and dynamic force microscopy

Figures 11(a)–11(f) show 5 μm square scans of the first, second, and seventh harmonic (a)–(c), and their phases (d)–(f), respectively, of PM on a mica surface. It is important to note that each higher-harmonic DFM image was obtained simultaneously while recording an attractive mode image by performing feedback in the usual way on the amplitude of the cantilever at ω_{B1}. Figure 11(a) [11(b)] is the conventional topography (phase) image of the mica substrate. A large aggregate of PM patches can be seen in the lower left half of the image. Measurements show two height levels at 5 nm and 10 nm above the mica substrate corresponding to one and two layers of PM. There is clear topographical contrast between mica, PM, and the PM double layer. Upon careful examination, a lipid deposit can be resolved in the topographic image [Fig. 11(a)] if the vertical scale is adjusted to increase height contrast. The lipid deposit was measured to be ~0.5 nm tall.

It is important to note the clear contrast between these different regions is also observed in the simultaneously acquired higher-harmonic maps. Because these experiments are performed in the amplitude feedback mode, the amplitude of the first bending mode is kept constant during the scans. Under this condition, contrast in the higher-harmonic signals then are entirely due to variations in the attractive forces over the sample. We note that the contrast between the second and seventh harmonic amplitudes is inverted, consistent with the report by Stark.[30]

Following the topography scan, dynamic force vs distance data were acquired over regions corresponding to mica, to dissociated lipids and to the PM. Representative dynamic force vs distance curves of the seventh harmonic (Fig. 12) indicate a far greater contrast between the PM, dissociated lipids, and the mica surface than those for the second harmonic (not shown). In fact using the Mikromasch NSC12 F cantilevers, the seventh harmonic provides by far the highest contrast between the three different regions comprising the sample. This implies that internally tuned cantilevers may

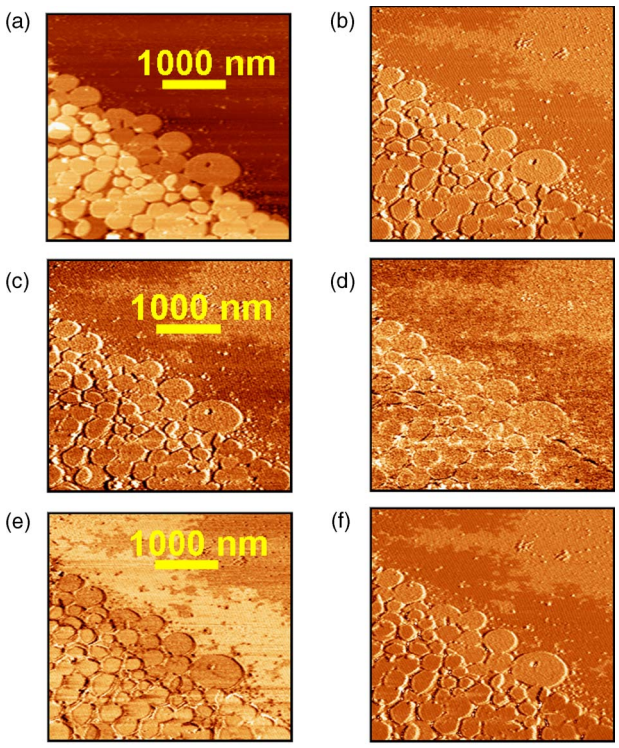

FIG. 11. (Color online) DFM topography and phase images of the PM deposited on mica. In (a) and (b), the usual amplitude and phase image taken while performing feedback on the amplitude when $\omega_d \cong \omega_{B1}$. An organized patch of PM (one and two layers high) is clearly resolved. In (c) and (d), an example of higher-harmonic DFM using the second harmonic images of amplitude and phase at $2\omega_d$ acquired simultaneously while acquiring the images in (a) and (b). In (e) and (f), an example of higher-harmonic DFM using the seventh harmonic image of amplitude and phase at $7\omega_d$. The higher-harmonic images clearly show contrast between a dissociated lipid "halo" surrounding the PM patch and the bare mica substrate.

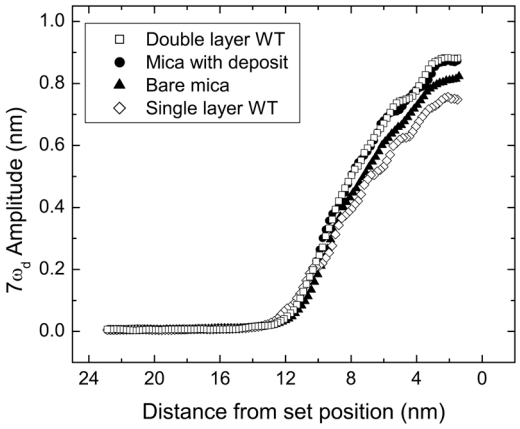

FIG. 12. The variation in amplitude of the seventh harmonic of the driving frequency vs tip-substrate separation when the tip is positioned over various regions on the PM sample and/or mica sample. The differences in amplitude observed during imaging (Fig. 11) are clearly visible.

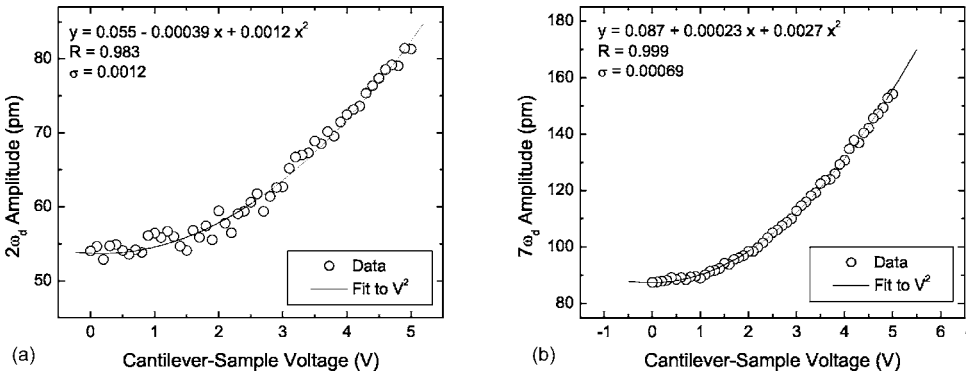

FIG. 13. Variation of the amplitude at $2\omega_d$ and $7\omega_d$ as a function of cantilever-substrate voltage. The amplitude at ω_{B1} was held constant while acquiring this data. In both cases, the observed variation can be well fitted by a second order polynomial.

amplify the effect of the interaction forces on the cantilever oscillations.[34] Clearly, the higher harmonics are sensitive indicators of the local attractive forces.

To further verify the effects reported above, all the above experiments were performed with a different model cantilever, an Olympus OMCL-A240TS-C1. For this cantilever, we found measurable signals at all harmonics up to the sixth. The sixth harmonic for this cantilever was reasonably close to the second bending mode frequency. The higher harmonic images and the dynamic force-distance curves using this Olympus cantilever showed contrast qualitatively similar to that obtained using the Mikromasch NSC12 cantilever reported above and provides evidence that this behavior is not unique in NSC12 cantilevers.

C. Influence of electrostatic forces

The connection between higher harmonics and the local van der Waals force explored in this paper is based on the assumption that this is the dominant contribution to the attractive interaction force. However biological macromolecules can be electrostatically charged, and it is not easy to decouple the effects of electrostatics from those of van der Waals forces. We now present experimental evidence that shows that the electrostatic forces in this system are negligible.

A sample of gold coated glass was inserted in the SFM and an NSC12 F cantilever was mounted and approached the sample in air at ambient humidity. The sample was approached in the standard manner and dynamic force vs distance data were acquired. The cantilever holder was grounded and the gold substrate was connected to a data acquisition card capable of producing 10 V dc output voltages. The voltage of the sample was ramped from 0 to 5 V and the output of the lock-in at the second and the seventh harmonic was acquired. Both the second and seventh harmonic signals clearly depend on the potential difference between the cantilever and the sample (Fig. 13). Both grow by $\sim$50% by the time the potential difference reaches 5 V.

To investigate whether there are negligible electrostatic forces between the tip and the PM sample, we consider the first bending mode dynamic force vs distance curve when the tip is above the gold surface. Figure 14(a) shows a set of data for this experimental configuration. For zero volts potential difference, the dynamic force-distance curve is reasonably flat far from the substrate and displays a sharp break point once the tip is close enough for tip-substrate forces to become significant. For a two volt potential difference, the dynamic force vs distance curve show a noticeably different behavior. The curve is bent out past the break point due to long range attractive forces between the cantilever and the substrate. When we compare this to the data set with the tip

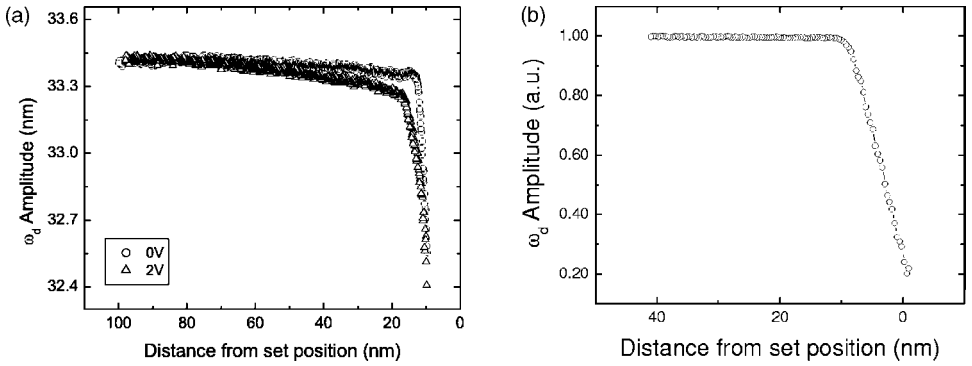

FIG. 14. Dynamic force-distance curves with various cantilever-sample potential differences. In (a), a comparison between the data acquired with 0 and 2 V applied to a gold substrate. The data clearly show bending for the 2 V case. In (b), the dynamic force-distance data obtained while taking images shown in Fig. 11 to show material contrast. The absence of bending at large tip-substrate separations implies no appreciable electrostatic effect.

over the PM (Fig. 14(b)), we see that no such bending is evident. We thus conclude that there is no direct evidence of large, electrostatic forces existing between the tip and PM samples. We therefore conclude that contrast due to van der Waals forces are the most likely cause of the observed differences in higher-harmonic signals between mica and PM.

VI. CONCLUSIONS

In this paper we present the theoretical background and experimental implementation of higher-harmonic dynamic force microscopy in the attractive regime. A theoretical model clearly shows that for a microcantilever oscillating in the attractive regime (a) the magnitudes of the higher harmonics are directly correlated to the local van der Waals forces assuming negligible electrostatic charging, (b) the higher harmonic peaks in the vibration spectrum are much sharper than for the fundamental harmonic, and (c) the frequency shifts in the *n*th harmonic are *n* times more sensitive to van der Waals forces compared to the primary harmonic. Systematic experiments have defined the conditions required to accurately observe higher-harmonic signals. The feasibility of higher-harmonic dynamic force microscopy is demonstrated using commercial microcantilevers to scan purple membrane deposited into mica. We observe systematic differences in the higher-harmonic dynamic force vs distance data over purple membrane, dissociated lipids, and mica.

This study suggests that systematic measurement of higher harmonics in the attractive regime can lead to highly sensitive maps of the chemical composition over heterogeneous nanostructures. Furthermore, using a higher harmonic as a feedback signal to image a substrate provides additional sensitivity for the *n*th harmonic due to the increasing sharpness of the higher-harmonic resonance peak. Taken together, these advantages offered by higher-harmonic dynamic force microscopy indicate that a wealth of new information can be accessed for the chemical and physical properties of nanoscale systems by implementing more advanced feedback detection schemes in scanning probe microscopy.

ACKNOWLEDGMENTS

Wild type bacteriorhodopsin was kindly provided by Professor Robert Birge's group at the University of Connecticut. The second author (A.R.) thanks the National Science Foundation for financial support for this research (Grants No. CMS 0116414 and No. CMS 0409660). The experimental work was partially supported by an ARO MURI Grant No. DAAD19-99-1-1098.

*Electronic address: scrittenden@arl.army.mil

[1] B. Anczykowski, D. Krüger, and H. Fuchs, Phys. Rev. B **53**, 15485 (1996).
[2] S. Hirsekorn, U. Rabe, and W. Arnold, Nanotechnology **8**, 57 (1997).
[3] J. P. Cleveland, B. Anczykowski, A. E. Schmid, and V. B. Elings, Appl. Phys. Lett. **72**, 2613 (1998).
[4] B. Anczykowski, B. Gotsmann, H. Fuchs, J. P. Cleveland, and V. B. Elings, Appl. Surf. Sci. **140**, 376 (1999).
[5] U. Dürig, New J. Phys. **2**, 1 (2000).
[6] E. Kester, U. Rabe, L. Presmanes, P. Tailhades, and W. Arnold, J. Phys. Chem. Solids **61**, 1275 (2000).
[7] M. Stark, R. W. Stark, W. M. Heckl, and R. Guckenberger, Appl. Phys. Lett. **77**, 3293 (2000).
[8] A. San Paulo and R. García, Phys. Rev. B **64**, 193411 (2001).
[9] M. Gauthier, N. Sasaki, and M. Tsukada, Phys. Rev. B **64**, 085409 (2001).
[10] S. I. Lee, S. W. Howell, A. Raman, and R. Reifenberger, Phys. Rev. B **66**, 115409 (2002).
[11] R. Boisgard, J. P. Aimé, and G. Couturier, Surf. Sci. **511**, 171 (2002).
[12] R. García and R. Pérez, Surf. Sci. Rep. **47**, 197 (2002).
[13] L. Nony, T. Cohen-Bouhacina, and J. P. Aimé, Surf. Sci. **499**, 152 (2002).
[14] A. San Paulo and R. García, Phys. Rev. B **66**, 041406(R) (2002).
[15] S. I. Lee, S. W. Howell, A. Raman, and R. Reifenberger, Ultramicroscopy **97**, 185 (2003).
[16] R. W. Stark, G. Schitter, and A. Stemmer, Phys. Rev. B **68**, 085401 (2003).
[17] C. Argento and R. H. French, J. Appl. Phys. **80**, 6081 (1996).
[18] B. Cappella and G. Dietler, Surf. Sci. Rep. **34**, 1 (1999).
[19] V. Snitka, A. Ulcinas, and V. Mizariene, Mater. Charact. **48**, 147 (2002).
[20] U. Rabe, M. Kopycinska, S. Hirsekorn, and W. Arnold, Ultrasonics **40**, 49 (2002).
[21] H. Hölscher, W. Allers, U. D. Schwarz, A. Schwarz, and R. Wiesenanger, Phys. Rev. Lett. **83**, 4780 (1999).
[22] A. S. Paulo and R. García, Surf. Sci. **471**, 71 (2001).
[23] S. N. Magonov, V. Elings, and M. H. Whangbo, Surf. Sci. Lett. **375**, L385 (1997).
[24] J. Tamayo and R. García, Appl. Phys. Lett. **71**, 2394 (1997).
[25] J. Tamayo and R. García, Appl. Phys. Lett. **73**, 2926 (1998).
[26] R. Hillenbrand, M. Stark, and R. Guckenberger, Appl. Phys. Lett. **76**, 3478 (2000).
[27] A. Sebastian, M. V. Salapaka, D. J. Chen, and J. P. Cleveland, J. Appl. Phys. **89**, 6473 (2001).
[28] O. Sahin and A. Atalar, Appl. Phys. Lett. **79**, 4455 (2001).
[29] A. Ulcinas and V. Snitka, Ultramicroscopy **86**, 217 (2001).
[30] R. W. Stark and W. M. Heckl, Rev. Sci. Instrum. **74**, 5111 (2003).
[31] S. Hu, S. Howell, A. Raman, R. Reifenberger, and M. Franchek, ASME J. Vibr. Acoust. **126**, 343 (2004).
[32] U. Dürig, Appl. Phys. Lett. **75**, 433 (1999).
[33] T. R. Rodriguez and R. Garcia, Appl. Phys. Lett. **84**, 449 (2004).
[34] O. Sahin, C. F. Quate, O. Solgaard, and A. Atalar, Phys. Rev. B **69**, 165416 (2004).
[35] T. R. Rodríguez and R. García, Appl. Phys. Lett. **80**, 1646 (2002).
[36] S. Hembacher, F. J. Giessibl, and J. Mannhart, Science **305**, 380 (2004).
[37] A. de Lozanne, Science **305**, 348 (2004).

[38] T. R. Rodríguez and R. García, Appl. Phys. Lett. **84**, 449 (2004).
[39] A. H. Nayfeh and D. T. Mook, *Nonlinear Oscillations* (Wiley, New York, 1995).
[40] O. Pfeiffer, C. Loppacher, C. Wattinger, M. Bammerliu, U. Gysin, M. Guggisberg, S. Rast, R. Bennewitz, E. Meyer, and H.-J. Güntherodt, Appl. Surf. Sci. **157**, 337 (2000).
[41] S. Sastry, *Nonlinear Systems: Analysis, Stability and Control* (Springer, New York, 1999).
[42] H. K. Khalil, *Nonlinear Systems*, 3rd ed. (Prentice-Hall, New York, 2002).
[43] B. M. Law and F. Rieutord, Phys. Rev. B **66**, 035402 (2002).
[44] M. Luna, J. Colchero, and A. M. Baró, Appl. Phys. Lett. **72**, 3461 (1998).
[45] T. Stifter, O. Marti, and B. Bhushan, Phys. Rev. B **62**, 13667 (2000).
[46] L. Zitzler, S. Herminghaus, and F. Mugele, Phys. Rev. B **66**, 155436 (2002).
[47] T. Schaffer and P. K. Hansma, J. Appl. Phys. **84**, 4661 (1998).
[48] T. E. Schaffer, J. Appl. Phys. **91**, 4739 (2002).
[49] R. W. Stark, G. Schitter, M. Stark, R. Guckenberger, and A. Stemmer, Phys. Rev. B **69**, 085412 (2004).
[50] T. E. Schaffer and H. Fuchs, J. Appl. Phys. **97**, 83524 (2005).
[51] R. Lévy and M. Maaloum, Nanotechnology **13**, 33 (2002).
[52] S. Rast, C. Wattinger, U. Gysin, E. Meyer, Nanotechnology **11**, 169 (2000).